Journal of Physics: Conference Series **702** (2016) 012008 doi:10.1088/1742-6596/702/1/012008

Many-body electron correlations in graphene

David Neilson[1], **Andrea Perali**[1] **and Mohammad Zarenia**[2]

[1] Dipartimenti di Fisica e di Farmacia, Università di Camerino, 62032 Camerino (MC), Italy
[2] Department of Physics, University of Antwerp, B-2020 Antwerpen, Belgium

E-mail: david.neilson@unicam.it

Abstract. The conduction electrons in graphene promise new opportunities to access the region of strong many-body electron-electron correlations. Extremely high quality, atomically flat two-dimensional electron sheets and quasi-one-dimensional electron nanoribbons with tuneable band gaps that can be switched on by gates, should exhibit new many-body phenomena that have long been predicted for the regions of phase space where the average Coulomb repulsions between electrons dominate over their Fermi energies. In electron nanoribbons a few nanometres wide etched in monolayers of graphene, the quantum size effects and the van Hove singularities in their density of states further act to enhance electron correlations. For graphene multilayers or nanoribbons in a double unit electron-hole geometry, it is possible for the many-body electron-hole correlations to be made strong enough to stabilise high-temperature electron-hole superfluidity.

1. Introduction

The Coulomb repulsion between conduction electrons in conventional metals and semiconductors affects their properties only through the relatively weak effects of linear screening and corrections to the values of the Landau Fermi liquid parameters. This is associated with the high densities of conduction electrons found in these materials. At such high densities, the Fermi energies are large or comparable to the average electron-electron interaction energies, and so the electrons behave as a weakly-interacting system. In such systems, many-body electron correlations are so weak that they play only a marginal role.

1.1. New phenomena for strongly correlated conduction electrons

If the density of conduction electrons could be lowered sufficiently to make electron interactions dominate over Fermi energies, a wealth of interesting new quantum phenomena driven by strong many-body electron correlations are predicted to appear. These phenomena include:

Wigner crystal of electrons

Charge density waves and other striped ground states

Metal-insulator transition

Quantum glass in the presence of defects

Coherent superconductor and electron-hole superfluid quantum states

Crossover from BCS superconductivity to Bose-Einstein condensation

1.2. When are many-body correlations expected to be important ?

A two-dimensional (2D) electron layer is expected to have correlations that are stronger than the correlations in a corresponding three- dimensional system at the same density, because of the smaller kinetic energy contributions. The dimensionless parameter r_s provides a measure of when electron correlations will be important. It is defined as $r_s = \langle PE \rangle / \langle KE \rangle$, and represents the relative importance of the average kinetic energy at zero temperature, $\langle KE \rangle = \langle \hbar^2 \nabla^2 / 2m^* \rangle \simeq \langle \hbar^2 / (m^* r_0^2) \rangle$, to the average strength of the Coulomb potential energy from electron repulsion, $\langle PE \rangle = \langle e^2 / \kappa r_0 \rangle$, where m^* is the electron effective mass and κ the dielectric constant of the background medium. For electrons of density n in a 2D layer, the average spacing between the electrons $r_0 = 1/\sqrt{\pi n}$. In a 2D system with parabolic dispersion of the energy bands, $r_s = r_0 / a_B^*$, where the effective Bohr radius for the system is $a_B^* = \kappa \hbar^2 / (e^2 m^*)$. Thus at sufficiently large r_0 (low electron densities), $r_s \gg 1$, and the electron Coulomb interactions will dominate over their Fermi energy.

2. Strongly correlated conduction electron systems

2.1. 2D Electron Liquid in Si MOSFETs and GaAs heterostructures

In 2D systems, the new phenomena driven by strong correlations are predicted to appear at very low densities, generally only for $r_s \gtrsim 10$ [1]. For many years quasi-2D electron layers at the interfaces of Si MOSFET devices and in narrow quantum wells in GaAs heterostructures (Fig. 1) have shown great promise as systems to access this low density region [2]. However even in the highest quality semiconductors with extremely high mobilities, residual defects and impurities still block much access to this interesting region, since when the electron density is lowered by metal gates or by doping, the samples always eventually become insulating. This electron freeze-out occurs when the remaining conduction electrons can no longer screen residual charged impurities and they become trapped by the impurities. The finite widths of the electron layers or quantum wells is a further challenge, as quantum wells must be wider than 10-15 nm in order to retain their good conduction properties. Finite widths mean weaker Coulomb interactions between electrons.

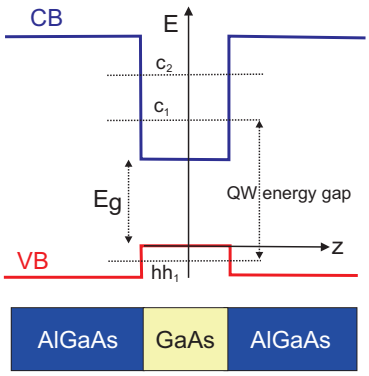

Figure 1. Quantum well in a GaAs heterostructure.

2.2. Graphene

In contrast to the quasi-2D electron layers in semiconductor systems, a graphene sheet is atomically flat and hence strictly 2D. There are no finite-width effects to weaken the Coulomb interactions. Levels of defects in graphene are extremely low so that electron freeze-out should be postponed to much lower electron densities.

2.2.1. Monolayer graphene

However nature has not been kind. Because the dispersion of the energy bands in monolayer graphene

is linear at low energies, $E_{\pm}(k) = \pm\hbar v_F k$ (Fig. 2), the Fermi energy $E_F = \hbar v_F k_F = \hbar v_F \sqrt{\pi n}$ and $\langle KE \rangle$ depend only linearly on r_0^{-1}. A result of this is that the $r_s = e^2/(\kappa \hbar v_F)$ in monolayer graphene does not depend on the electron density. The Fermi velocity $v_F \simeq 10^6$ ms^{-1} and the dielectric constant of the substrate is typically $\kappa \sim 3$ [3], making the fixed value of r_s small, $r_s \sim 0.5$-0.7. Such a small value for r_s implies that the correlations of the conduction electrons in monolayer graphene will always remain weak [4].

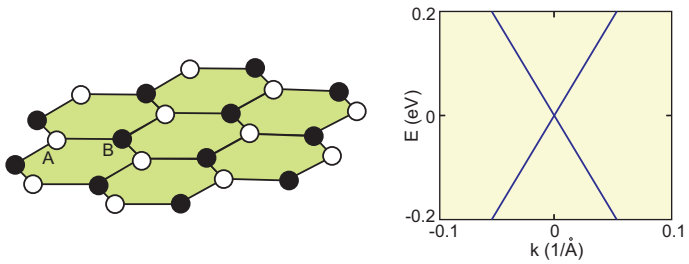

Figure 2. Monolayer graphene: atomic structure and linear energy bands at low energies.

2.2.2. Bilayer graphene

It should, nevertheless, be possible to access the strongly correlated region in graphene. One work-around is to substitute a graphene bilayer sheet in place of the graphene monolayer. A symmetrically biased graphene bilayer with AB stacking is a semiconductor with parabolic dispersion of the energy bands [5] (Fig. 3). With parabolic dispersion, the interaction parameter r_s once again increases with decreasing electron density as it does in a semiconductor system [6]. Furthermore, in contrast to monolayer graphene, if a perpendicular electric field is applied across bilayer graphene using a metal gate, the field will generate a tuneable energy gap between the conduction and valence bands.

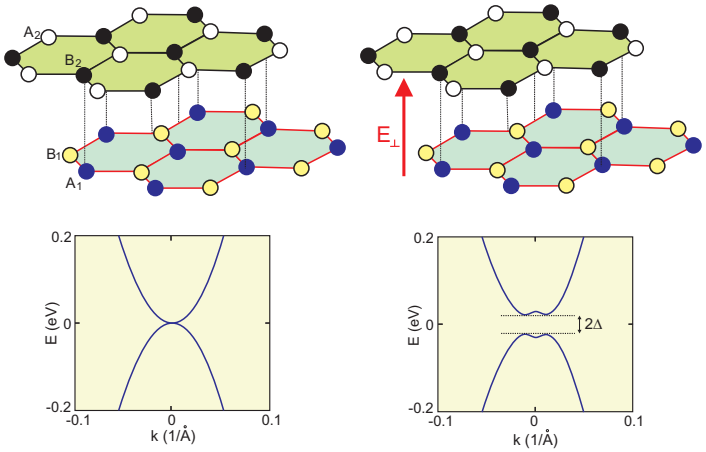

Figure 3. Bilayer graphene: atomic structure and parabolic energy bands at low energies. With an external perpendicular electric field $E_{\perp}$ there is an energy gap 2Δ between the valence and conduction bands.

The low density regime in bilayer graphene is dominated by disorder in current samples, making a lower limit for the electron density of $n \sim 10^{10}$ cm^{-2}, corresponding to a large maximum value for

$r_s = 23$. At very low densities a trigonal warping of the bands could transform the parabolic bands into sets of Dirac-like linear bands [7], but residual disorder will mask this effect, and it could be further reduced if necessary by applying an electric field to open up an energy band gap.

In summary, extreme high quality, atomically flat bilayer graphene sheets have tuneable electron densities and band gaps that should permit the bilayers to readily access new quantum phenomena predicted for strong electron correlations.

2.2.3. Few-layer graphene

Increasing the number of graphene layers in the sheet beyond bilayers greatly enhances the density of states (DOS), and this projects the sheets even more dramatically into the region of strong correlations at accessible densities [8]. Electron graphene multilayers should be able to access regions of phase space with very strong electron-electron interactions. For the lowest energy band in ABC stacked N-layer graphene, the energy dispersion of the conduction band is given by [9, 10],

$$E^{(N)}(k) = \left\{(\hbar v_F)^N / t^{N-1}\right\} k^N \ , \tag{1}$$

where $t \approx 400$ meV is the interlayer hopping term in few-layer graphene. Figure 4(a) shows $E^{(N)}(k)$ for $N = 1$ to 4. Using Eq. (1) to determine the Fermi energy E_F at density n, we obtain for N-layer graphene,

$$r_s = \langle PE \rangle / \langle KE \rangle = \left\{ \frac{e^2 t^{N-1}}{\kappa (\hbar v_F)^N \sqrt{\pi^{N-1}}} \right\} \frac{1}{n^{(N-1)/2}} \ . \tag{2}$$

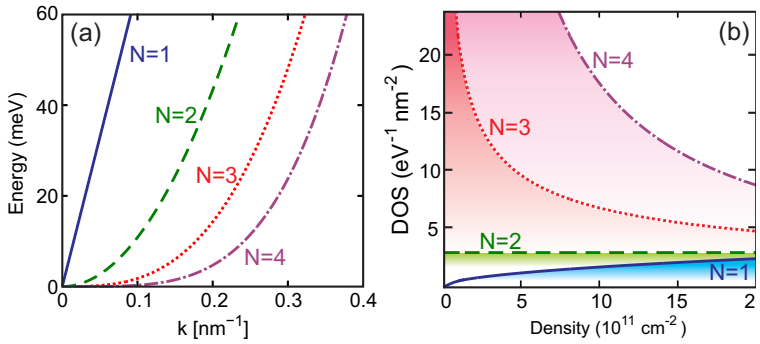

Figure 4. (a) Lowest positive energy band in monolayer ($N = 1$), bilayer ($N = 2$), trilayer ($N = 3$), and quadlayer ($N = 4$) graphene. (b) Comparison for $N = 1$ to $N = 4$ of the density of states at the Fermi energy $DOS^{(N)}(E_F)$ as function of electron density [8]. The van Hove power law singularities as $E_F \to 0$ lead to large enhancements of the DOS for trilayer and quadlayer graphene.

A consequence of the different energy dispersions $E^{(N)}(k)$ is that the dependence of the density of states on energy changes dramatically with the number of layers N,

$$DOS^{(N)}(E) = \frac{d\Omega^{(N)}}{dE} = \frac{2\pi}{N} \frac{t^{2(N-1)/N}}{(\hbar v_F)^2} E^{(2/N)-1} \ , \tag{3}$$

where $\Omega^{(N)}(k)$ is the volume in k-space of the N-layer sheet. Figure 4(b) shows the dependence of $DOS^{(N)}(E_F)$ at the Fermi energy on electron density n. For monolayer graphene $DOS^{(1)}(E_F)$ depends linearly on n, for bilayer graphene $DOS^{(2)}(E_F)$ is a constant, and for trilayer and quadlayer graphene $DOS^{(N)}(E_F)$ decreases with increasing n. Because of the van Hove singularities as $E \to 0$, the $DOS^{(3)}(E_F)$ and $DOS^{(4)}(E_F)$ for small densities are much larger than $DOS^{(1)}(E_F)$

Density (cm^{-2})	monolayer	bilayer	trilayer	quadlayer
5×10^{12}	0.7	1	2	3
1×10^{12}	0.7	3	8	29
5×10^{11}	0.7	4	17	83
1×10^{11}	0.7	8	86	930

Table 1. Values of the interaction parameter r_s for few-layer graphene as a function of electron density. Large values of $r_s \gg 1$ can lead to new phases driven by the strong electron correlations.

and $DOS^{(2)}(E_F)$. Eventually, at very high densities lying well outside our range of interest, the $DOS^{(3)}(E_F)$ and $DOS^{(4)}(E_F)$ are smaller than $DOS^{(1)}(E_F)$ and $DOS^{(2)}(E_F)$.

Table I compares the values of r_s for the typical electron densities found in graphene sheets for N-layer graphene, for $N = 1$ (monolayer) to $N = 4$ (quadlayer). The table shows that few-layer graphene offers dramatic opportunities for producing extremely strongly interacting electron systems at experimentally accessible densities.

Experimental realisation of few layer graphene is within the grasp of current technology since few-layer graphene sheets can be fabricated in large areas by both mechanical exfoliation [11, 12] and by chemical techniques [13, 14, 15] from graphite with controlled stacking order. References [16, 17, 18] are examples of experimental studies on electronic and transport properties in trilayer graphene.

2.2.4. Graphene nanoribbons

Electrons can be confined in nanoribbons that are only a few nanometres in width, etched on monolayers of graphene. The nanoribbons can have multiple energy subbands that are occupied. Their electronic properties depend on the type of edge termination [19]. We discuss here only armchair-edge terminated graphene nanoribbons (Fig. 5), since, unlike for zig-zag-edge terminated nanoribbons, the multiple subbands of armchair nanoribbons are parabolic around their minima and there is a semiconductor-like energy gap between conduction and valence bands (Fig. 5). Also, there is no valley degeneracy. These properties all act to diminish the effect of Coulomb screening. Uniform armchair graphene nanoribbons of widths much less than 10 nm have already been fabricated [20].

Electron correlations in armchair-edge terminated nanoribbons will be further boosted by the quantum confinement of the electrons along the nanoribbons, and also by quantum size effects and van Hove singularities in the quasi-one-dimensional density of states that are accessed if the Fermi energy is increased so it enters the bottom of a new subband.

Figure 5 shows the single-particle energy subbands j in the continuum model, $\epsilon_j(k_y) = (\sqrt{3}ta_0/2)\sqrt{k_y^2 + k_j^2},\ j = 1, 2, \ldots$ for an armchair graphene nanoribbon of width $W = 2$ nm, where $t = 2.7$ eV is the intralayer hopping energy [21] and $a_0 = 0.24$ nm is the graphene lattice constant. We take the y-direction parallel to the nanoribbon, with the electrons confined in the transverse x-direction. The quantised wave-number for the j-subband in the x-direction is $k_j = [j\pi/W] - \left[4\pi/(3\sqrt{3}a_0)\right]$. The lower panels in Figure 5 show the corresponding density of states DOS(E). The van Hove singularities are clearly visible at the bottom of each subband.

2.3. Graphene in a periodic magnetic field

A periodic magnetic field applied perpendicular to the graphene monolayers can preserve the isotropic Dirac cones of the monolayer energy bands while reducing the slope of the Dirac cones [23, 24, 25, 26]. We represent the magnetic field perpendicular to the monolayer as a one-dimensional array with period $2d$ of successive rectangular magnetic barriers and wells of height $B_z = \pm B$ and dimensionless width $d = d_B/\ell_B$, where $\ell_B = \sqrt{\hbar c/eB}$ is the magnetic length. Since the average of the magnetic flux across a unit cell of the periodic field is fixed at zero, the main effect of the magnetic field is to modify the

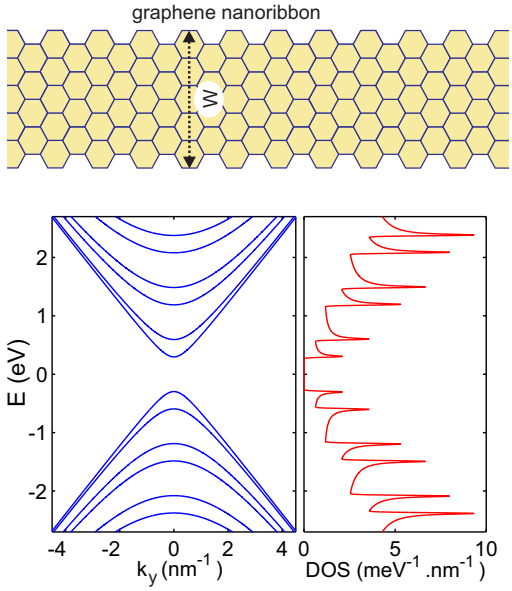

Figure 5. Top: armchair-edge terminated graphene nanoribbon of width W. Lower panels: lowest single-particle energy subbands $\epsilon_j(k_y), j = 1, 2, \ldots$ for an armchair nanoribbon of width $W = 2$ nm, and corresponding density of states DOS(E) in the nanoribbon [22]. Van Hove singularities are visible at the bottom of each subband.

electronic band structure of the graphene monolayers. In this field, the single-particle energy dispersion of the monolayer graphene remains linear, but the velocity $\alpha_d v_F$ is less than the original Fermi velocity v_F, so

$$\epsilon(\mathbf{k}) = \pm\hbar(\alpha_d v_F)|\mathbf{k}|\,(1 + \delta(\mathbf{k}))\ . \tag{4}$$

The non-linear correction term $\delta(\mathbf{k})$ is small, with $|\delta(\mathbf{k})| \lesssim d_B^2 k_x^2/6$. The constant $\alpha_d \leq 1$, representing the decrease in the Fermi velocity, depends on d [23, 26],

$$\begin{aligned} \alpha_d &\simeq 1 - d^4/60 \qquad d \ll 1 \\ \alpha_d &\simeq \tfrac{2d}{\sqrt{\pi}} e^{-d^2/4} \qquad d \gg 1\ . \end{aligned} \tag{5}$$

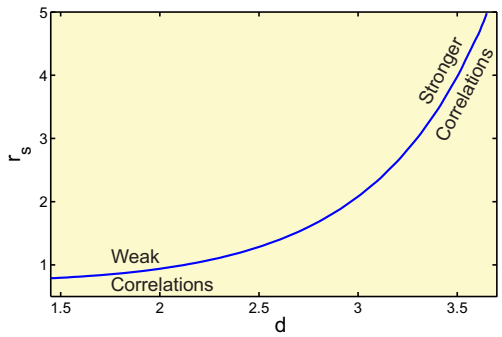

Figure 6. Variation of the interaction parameter r_s for monolayer graphene in a perpendicular magnetic field of periodicity $2d = 2d_B/\ell_B$ (see text). Without the magnetic field, r_s is a constant less than unity, and is independent of electron density.

Recalling for graphene monolayers that the density-independent interaction strength parameter is $r_s = e^2/(\kappa\hbar v_F)$, we see that an effect of the reduction of the Fermi velocity in Eq. 4 is to increase the value of the r_s parameter by a factor α_d^{-1}. Figure 6 shows that we can significantly increase r_s by using the periodic magnetic field to tune α_d with d.

3. Electron-hole superfluidity in graphene

Two graphene monolayers of electrons and holes separated by a very thin insulating barrier has been proposed to observe an electron-hole superfluid [27, 28, 29]. A hexagonal boron nitride (hBN) separation barrier as thin as 1 nm can efficiently insulate the two monolayers from each other [30]. However, theory suggests that because of strong screening of the electron-hole pairing interaction, an electron-hole superfluid can only occur when $r_s > 2.3$ [31]. Experiments confirm that the superfluid is not seen in two graphene monolayers [30], where we recall r_s is fixed independent of density at $r_s \sim 0.5$-0.7.

This poses a challenge as to whether new structures can be designed and fabricated using atomically thin crystals, structures in which a superfluid transition can be observed. The graphene sheets discussed in Sections 2.2.2 to 2.2.4 can all access the region $r_s \gg 2.3$, and hence they constitute promising candidates to generate this elusive electron-hole superfluid [6, 8, 32, 33].

In superfluid systems in graphene, it would be straightforward to access the BCS-BEC crossover and BEC regimes using the electric potential on metal gates and by tuning the sample parameters. This possibility opens up interesting new connections with the physics of ultracold fermions and high-T_c superconductors.

We have predicted the existence of electron-hole superfluidity in the graphene structures described in Sections 2.2.2 to 2.2.4. We find mean field zero temperature superfluid gaps that are consistently large, of the order of several hundred Kelvin. Unlike in three-dimensions, however, the superfluid phase transition temperature T_c in a two-dimensional system is not related linearly to the magnitude of its zero temperature superfluid gap. For quantum condensates in two-dimensions, an upper bound on the transition temperature is the Kosterlitz-Thouless temperature [34], $T_{KT} = (\pi/2)J(T_{KT})$, where $J(T)$ is the average kinetic energy of the Cooper pairs. At zero temperature, $J(0)$ is proportional to the superfluid density, $J(0) = \rho_s(0)/2$, and, since in mean field $\rho_s(T)$ depends very weakly on temperature for T small compared with the zero-temperature superfluid gap, for this case we may approximate $J(T)$ by $J(0)$ [35].

We find the resulting T_{KT} is typically of order 15 K for the electron-hole coupled graphene bilayers and the electron-hole coupled graphene monolayers in a periodic magnetic field, for sheet separations ~ 2 nm and typical experimental carrier densities, $n \sim 10^{12}$ cm^{-2}. Switching from coupled electron-hole bilayers to the coupled electron-hole quadlayers for the same sheet separation, typically doubles the T_{KT}. These results indicate that electron-hole superfluidity should be readily detectable in these graphene structures using existing technology.

4. Conclusions

With graphene and related atomically thin crystals, we are at an exciting many-body threshold to realise and exploit novel quantum phases with tuneable properties. High quality, atomically flat two-dimensional electron graphene sheets and quasi-one-dimensional electron graphene nanoribbons with tuneable electron densities and band gaps, should exhibit novel phenomena driven by strong many-body correlations. These phenomena are predicted when Coulomb repulsions between electrons are dominant over their Fermi energies, and include the Wigner crystal and charge density waves. In addition, certain configurations of double graphene sheets or nanoribbons, one doped with electrons and one with holes, should generate an electron-hole superfluid state characterised by a very large superfluid energy gap and relatively high transition temperature.

Acknowledgments
We thank Lucian Covaci and François Peeters (University of Antwerp), Alexander Hamilton (University of New South Wales), and Luca Dell'Anna (University of Padua) for useful discussions. We acknowledge support by the University of Camerino FAR project CESEMN (DN and AP), the Flemish Science Foundation (FWO-Vl) (MZ) and the University of Antwerp Research Fund (BOF) (MZ). The authors thank colleagues involved in the MultiSuper International Network (http://www.multisuper.org) for exchange of ideas connected with this work.

References
[1] Świerkowski L, Neilson D, and Szymański J 1991 Phys. Rev. Lett. **67**, 240; Rapisarda Francesco and Senatore Gaetano 1996 Aust. J. Phys. **49**, 161
[2] Zheng B, Croxall A F, Waldie J, Das Gupta K, Sfigakis F, Farrer I, Beere H E, Ritchie D A 2015 ArXiv:1511.08701
[3] Young A F, Dean C R, Meric I, Sorgenfrei S, Ren H, Watanabe K, Taniguchi T, Hone J, Shepard K L and Kim P 2012 Phys. Rev. B **85**, 235458
[4] Dahal Hari P, Joglekar Yogesh N, Bedell Kevin S, Balatsky Alexander V 2006 Phys. Rev. B **74**, 233405; Das Sarma S, Adam Shaffique, Hwang E H and Rossi Enrico 2011 Rev. Mod. Phys. **83**, 407
[5] McCann E and Fal'ko V I 2006 Phys. Rev. Lett. **96**, 086805
[6] Perali A, Neilson D and Hamilton A R 2013 Phys. Rev. Lett. **110**, 146803
[7] Castro Neto A H, Guinea F, Peres N M R, Novoselov K S and Geim A K 2009 Rev. Mod. Phys. **81**, 109
[8] Zarenia M, Perali A, Neilson D and Peeters F M 2014 Sci. Reports **4**, 7319
[9] Min H and MacDonald A H 2008 Phys. Rev. B **77**, 155416
[10] Katsnelson, M I 2012 *Graphene: Carbon in two dimensions* (New York: Cambridge University Press)
[11] Ferrari A C, Meyer J C, Scardaci V, Casiraghi C, Lazzeri M, Mauri F, Piscanec S, Jiang D, Novoselov K S, Roth S and Geim A K 2006 Phys. Rev. Lett. **97**, 187401
[12] Zhang Y, Small J P, Pontius W V and Kim Philip 2005 Appl. Phys. Lett. **86**, 073104
[13] Berger C, Song Z, Li T, Li X, Ogbazghi A Y, Feng R, Dai Z, Marchenkov A N, Conrad E H, First P N and de Heer W A 2004 J. Phys. Chem. B **108**, 19912
[14] Shih Chih-Jen, Vijayaraghavan A, Krishnan R, Sharma R, Han Jae-Hee, Ham Moon-Ho, Jin Zh, Lin Sh, Paulus G L C, Reuel N F, Wang Q H, Blankschtein D and Strano M S 2011 Nature Nanotechnology **6**, 439
[15] Mahanandia P, Simon F, Heinrich G and Nanda K K 2014 Chem. Commun. **50**, 4613
[16] Craciun M F, Russo S, Yamamoto M, Oostinga J B, Morpurgo A F and Tarucha S 2009 Nature Nanotech. **4**, 383
[17] Bao W, Jing L, Velas J, Aykol M, Cronin S B, Smirnov D, Koshino M, McCann E, Bockrath M and Lau C N 2011 Nature Phys. **7**, 948
[18] Mak Kin Fai, Shan Jie and Heinz Tony F 2010 Phys. Rev. Lett. **104**, 176404
[19] Brey L and Fertig H A 2007 Phys. Rev. B **75**, 125434
[20] Tapasztó L, Dobrik G, Lambin P and Biró L P 2008 Nature Nanotechnology **3**, 397
[21] Brey L and Fertig H A 2006 Phys. Rev. B **73**, 235411
[22] Zarenia M, Perali A, Peeters F M and Neilson D 2015 ArXiv:1601.06942
[23] Dell'Anna L and De Martino A 2009 Phys. Rev. B **79**, 045420; *ibid.* 2009 **80**, 089901(E)
[24] Snyman I 2009 Phys. Rev. B **80**, 054303
[25] Tan L Z, Park C -H and Louie S G 2010 Phys. Rev. B **81**, 195426
[26] Dell'Anna L and De Martino A 2011 Phys. Rev. B **83**, 155449
[27] Zhang C -H and Joglekar Y N 2008 Phys. Rev. B **77**, 233405; Lozovik Yu E and Sokolik A A 2008 JETP Lett. **87**, 55; 2010 Eur. Phys. J. B **73**, 195; Mink M P, Stoof H T C, Duine R A and MacDonald A H 2011 Phys. Rev. B **84**, 155409
[28] Min Hongki, Bistritzer Rafi, Su Jung-Jung and MacDonald A H 2008 Phys. Rev. B **78**, 121401(R)
[29] Bistritzer R, Min H, Su J -J and MacDonald A H 2008 ArXiv:cond-mat/0810.0331v1
[30] Gorbachev R V, Geim A K, Katsnelson M I, Novoselov K S, Tudorovskiy T, Grigorieva I V, MacDonald A H, Watanabe K, Taniguchi T and Ponomarenko L A 2012 Nat. Phys. **8**, 896
[31] Lozovik Yu E, Ogarkov S L and Sokolik A A 2012 Phys. Rev. B **86**, 045429
[32] Neilson D, Perali A and Hamilton A R 2014 Phys. Rev. B **89**, 060502(R)
[33] Dell'Anna L, Perali A, L Covaci L and Neilson D 2015 Phys. Rev. B **92** 220502(R)
[34] Kosterlitz J M and Thouless D J 1973 J. Phys. C: Sol. State Phys., **6**, 1181
[35] Benfatto L, Capone M, Caprara S, Castellani C, and Di Castro C 2008 Phys. Rev. B **78**, 140502(R); Benfatto L and Sharapov S G 2006 Low Temp. Physics **32**, 533